Available online at www.eccomasproceedia.org
Eccomas Proceedia COMPDYN (2023) 4439-4450

ECCOMAS
Proceedia

COMPDYN 2023
9th ECCOMAS Thematic Conference on
Computational Methods in Structural Dynamics and Earthquake Engineering
M. Papadrakakis, M. Fragiadakis (eds.)
Athens, Greece, 12-14 June 2023

RAILWAY TRACK STRUCTURAL DYNAMICS VIA PERIODIC APPROACHES

Angie C. Lamprea-Pineda[1], Alexandre Castanheira-Pinto[2], Pedro Alves Costa[2], Peter K. Woodward[1], Mohammed F.M. Hussein[3], and David P. Connolly[1]

[1] Institute for High Speed Rail and System Integration, University of Leeds
LS29JT, Leeds, UK
e-mail: {cnaclp@leeds.ac.uk, D.Connolly@leeds.ac.uk, P.K.Woodward@leeds.ac.uk}

[2] Construct-FEUP, University of Porto
4099-002, Porto, Portugal
e-mail: {amgcpinto@fe.up.pt, pmbcosta@reit.up.pt}

[3] Department of Civil and Architectural Engineering, Qatar University
2713 Doha-Qatar
e-mail: {mhussein@qu.edu.qa}

Abstract

Periodicity can be defined as the repetitive character of a structure's features. In railway track systems, periodicity can be found in the geometrical and material properties in the train passage direction. For example, the repeating pattern of sleepers, rail seats or slab track units. To take advantage of this, this paper employs the direct periodic method, a novel numerical method which exploits the invariant nature of the railway track structure. Instead of simulating the total track domain, the direct periodic method studies a discrete portion of the track, often known as the reference cell, which captures its repetitive pattern and provides the total track response. First, the cell response is obtained by enforcing compatibility conditions within its system of equations of motion in the wavenumber-frequency domain. Then, the total space response is retrieved by replicating the cell's solution via a combination of periodic conditions and Fourier transformations. It is combined with perfectly matched layers to simulate infinite depth soil boundary conditions. Thus, this paper employs the direct periodic method in combination with perfectly matching layers to analyze track-ground dynamic interaction.

Keywords: Periodic Modelling, Ballasted Track, Vibration Problems, Vibration Modes, Wave Propagation, Frequency Response.

ISSN:2623-3347
Peer-review under responsibility of the organizing committee of COMPDYN 2023.
doi: 10.7712/120123.10731.21028

1 INTRODUCTION

Vibration issues in railway systems are a result of the intricate dynamic relationship between the train, the track, and the supporting soil. As the need for transportation increases, so does the severity of these problems, requiring an in-depth comprehension of the dynamic behavior of the system components, improved design, and efficient solutions to reduce future maintenance and replacement costs. Consequently, assessing the condition of the entire system and its components is essential.

Often, this characterization is accomplished through empirical, analytical, semi-analytical, and numerical methods that enable the simulation and assessment of vibration issues associated with railway systems. The first approach is usually limited to specific conditions and is based on experience, numerical data, and field results for its formulation [1,2]. Perhaps the most comprehensive studies on railway track components' behavior have been conducted using analytical methods involving beam-on elastic foundation (BOEF) formulations. These studies have a straightforward definition which simplifies the components of the track system into beams, elastic elements, and lumped masses. Thus, allowing for a broad range of analyses – see for instance [2,3,4,5].

However, analytical approaches find it challenging to represent wave propagation in complex geometries. To overcome this limitation, the soil behavior is approximated using stiffness and flexibility matrices defined in the frequency domain. Examples of this are the domain transformation (DT) by Sheng [6,7] and the thin-layer method (TLM) [8]. Despite their accuracy, analytical and semi-analytical approaches cannot represent complex geometries. This has led to the development of numerical methods such as finite element methods (FEM), which provides a more flexible description of railway system behavior (e.g. complex railhead geometries, transition zones, etc. [9,10,11]). However, these methods require significant computational capacity due to the need for large domains.

Alternatively, periodic methods are implemented to reduce the computational effort while still providing accurate approximations of the structure's behavior. These methods exploits the periodic or repetitive characteristics of the structure (e.g. material and geometrical properties), allowing for a reduction of the domain under consideration and consequently, providing lower computational times [12,13,14,15]. In railway systems, the behavior is observed in both ballast and slab tracks. For instance, in ballasted tracks, the pattern is given by the repeated sleeper arrangement [16,17]; whereas in slab tracks, this is generated by the discrete rail-seats or repeating slab units [18,19,20,21]. Among the various periodic approaches, the 2.5D FEM has been extensively used for train-track-ground simulations in recent years [22,23,24,25,26,27]. Typically, this method is coupled with BE or PML (perfectly matching layers [28]) to account for the wave propagation response. However, the 2.5D FE only defines the structure's cross-section and assumes a homogenous behavior in the longitudinal direction, which makes it unable to represent the discrete support effect.

The periodic approach proposed by [29], known as the direct periodic method (DM), can address the limitation of computing the response of discretely supported structures. This method obtains the system's response via a direct inversion of a modified equilibrium formulation in the wavenumber-frequency domain. By combining it with PML, the DM allows to simulate infinite depth soil boundary conditions and further improving the efficiency of the overall computation.

Thus, this paper employs the direct periodic approach in combination with perfectly matching layers in order to study the dynamic behavior of a periodic ballasted track resting on a homogeneous ground.

2 MODELLING APPROACH

The direct periodic method (DM) defined by [29], in combination with 3D finite elements and perfectly matching layers (3D FE-PML), is employed in the simulation of the train-track-ground interaction response. By enforcing the periodic characteristic of the ballasted tracks, the DM allows to retrieve the behavior of the total domain (Ω) via the analysis of a restricted domain of length d – also referred to as the unit or reference cell ($\widetilde{\Omega}$), which is assumed to infinitely repeat itself in the longitudinal or direction x – see Figure 1. This allows for the formulation and solution of the system of equations of motions, in the wavenumber and frequency domain (k_1, ω), in terms of $\widetilde{\Omega}$. Then, by enforcing periodic conditions and Fourier transformations, the response of Ω is retrieved in the space domain.

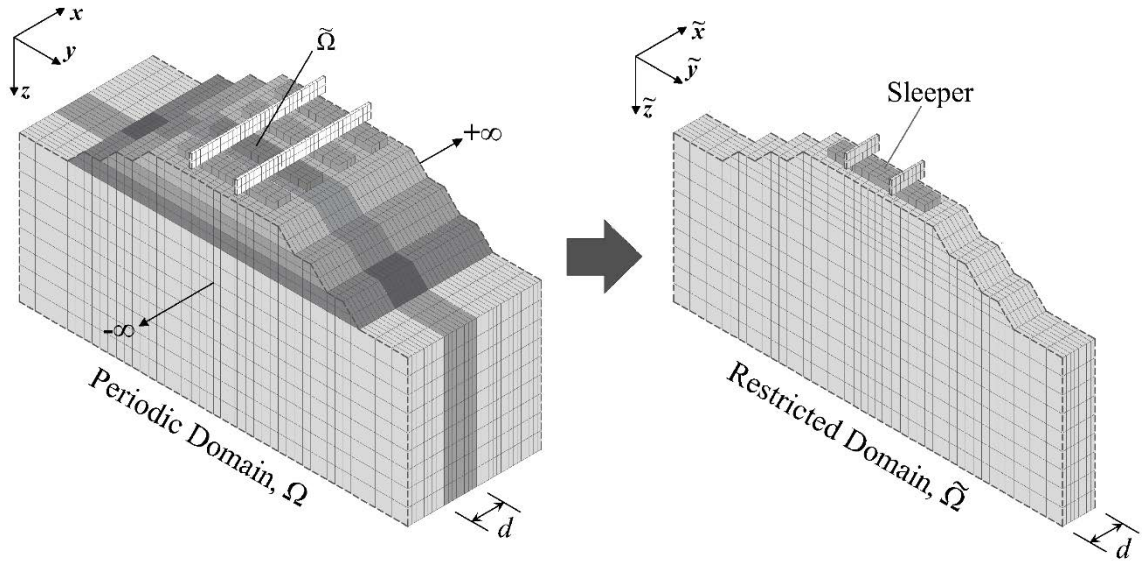

Figure 1: Periodic ballasted track domain infinitely extending in the longitudinal direction and its reference cell of length d.

2.1 Reference cell definition

The track and the ground behavior are included in the reference cell's formulation – as shown in Figure 1. In the first case, FE are employed. In contrast, PML are used to define the wave propagation effect of the ground. Then, both are coupled within a dynamic stiffness matrix (DSM) which allows for the definition of the system of equations of motion of $\widetilde{\Omega}$ - as described in Equation (1):

$$\left[\widetilde{D}_{n=0}\right]\{\tilde{u}_{n=0}\} = \{\tilde{F}_{n=0}\} \tag{1}$$

where $\{\tilde{u}_{n=0}\}$ and $\{\tilde{F}_{n=0}\}$ are the vectors of displacements and forces of $\widetilde{\Omega}$, respectively. The DSM, $\left[\widetilde{D}_{n=0}\right]$ (Equation (2)), is defined by the matrices of mass $[M_{n=0}]$ and complex stiffness $[K_{n=0}]$, the latter accounting for a hysteretic damping model (Equation (3)).

$$\left[\widetilde{D}_{n=0}\right] = [K_{n=0}] - \omega^2[M_{n=0}] \tag{2}$$

$$[K_{n=0}] = [k_{n=0}](1 + i\eta) \tag{3}$$

where $[k_{n=0}]$ is the matrix of stiffness and η is the damping loss factor. Note that when accounting for the ground representation, the PML uses complex stretching coordinates, which

are defined upon complex stretching functions $\tilde{\lambda}_{\tilde{s}}$. Thus, the matrices in Equations (2)-(3) are also complex and described by:

$$\begin{aligned}\left[k_{n=0}^{PML}(\tilde{x},\tilde{\lambda}_{\tilde{y}},\tilde{\lambda}_{\tilde{z}})\right] &= \int_{\tilde{x}}\int_{\tilde{y}}\int_{\tilde{z}}\tilde{\lambda}_{\tilde{y}}\tilde{\lambda}_{\tilde{z}}\left[\check{B}(\tilde{x},\tilde{\lambda}_{\tilde{y}},\tilde{\lambda}_{\tilde{z}})\right]^{T}[D]\left[\check{B}(\tilde{x},\tilde{\lambda}_{\tilde{y}},\tilde{\lambda}_{\tilde{z}})\right]d\tilde{x}d\tilde{y}d\tilde{z}\\ \left[M_{n=0}^{PML}(\tilde{x},\tilde{\lambda}_{\tilde{y}},\tilde{\lambda}_{\tilde{z}})\right] &= \int_{\tilde{x}}\int_{\tilde{y}}\int_{\tilde{z}}\tilde{\lambda}_{\tilde{y}}\tilde{\lambda}_{\tilde{z}}\left[\check{N}(\tilde{x},\tilde{\lambda}_{\tilde{y}},\tilde{\lambda}_{\tilde{z}})\right]^{T}\rho\left[\check{B}(\tilde{x},\tilde{\lambda}_{\tilde{y}},\tilde{\lambda}_{\tilde{z}})\right]d\tilde{x}d\tilde{y}d\tilde{z}\end{aligned} \quad (4)$$

where $\left[\check{B}(\tilde{x},\tilde{\lambda}_{\tilde{y}},\tilde{\lambda}_{\tilde{z}})\right]$ is the complex matrix of partial derivatives of the shape functions $\left[\check{B}(\tilde{x},\tilde{\lambda}_{\tilde{y}},\tilde{\lambda}_{\tilde{z}})\right]$, and $[D]$ is the material matrix. Note that in the case of FEM, $\tilde{\lambda}_{\tilde{s}}=1$.

2.2 Compatibility conditions and solution

To allow for continuity of the displacements and equilibrium of forces between each repeated cell, periodic conditions, formulated upon the Floquet's theorem [30], must be enforced within the reference cell boundaries:

$$\tilde{u}_n(x,y,z,k_1,\omega)=\tilde{u}_{n=0}(\tilde{x},\tilde{y},\tilde{z},k_1,\omega)e^{ik_1nd} \quad (5)$$

in where $\tilde{u}_n$ and $\tilde{u}_{n=0}$ are the displacements of the complete and discretized domain, respectively. Similarly, the space vectors in Ω and $\tilde{\Omega}$ are defined by $s=\{x,y,z\}$ and $\tilde{s}=\{\tilde{x},\tilde{y},\tilde{z}\}$, respectively; the cell number is defined by n, being *n=0* and *n≠0* the reference and the remaining cells. Overall, the tilde notation '~' represents the transformed domain (k_1,ω), corresponding to the wavenumber k_1 and angular frequency ω. To impose Equation (5), the reference cell's displacements at its front ($\tilde{u}_{n=0}^{front}$) and back face ($\tilde{u}_{n=0}^{back}$) must be related through the exponential term e^{ik_1d}:

$$\tilde{u}_{n=0}^{front}(\tilde{x}=d,\tilde{y},\tilde{z},k_1,\omega)=\tilde{u}_{n=0}^{back}(\tilde{x}=0,\tilde{y},\tilde{z},k_1,\omega)e^{ik_1d} \quad (6)$$

where $\tilde{u}_{n=0}^{front}$ and $\tilde{u}_{n=0}^{back}$ refer to the front and back border displacements of the reference cell, respectively – see Figure 2. Equation (6) ensures continuity at the boundaries of every n^{th} cell.

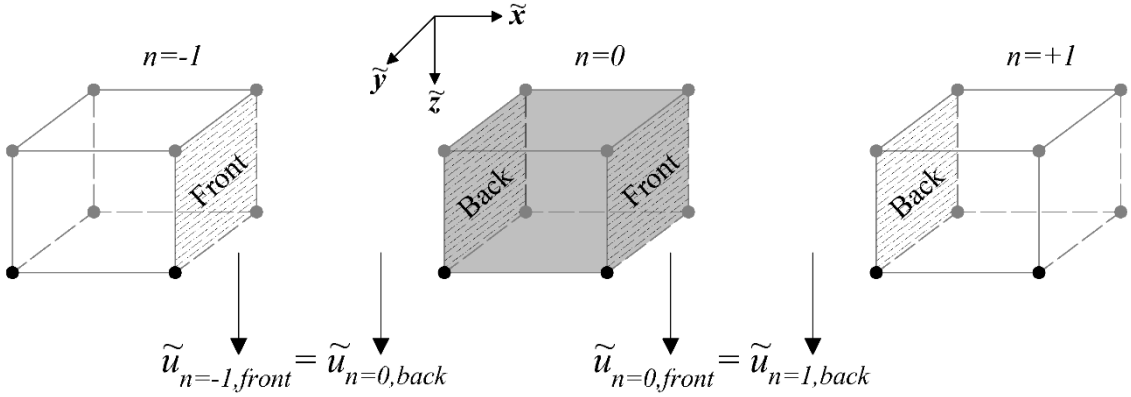

Figure 2: Continuity of displacements at the boundaries of the cells.

Once the displacements in all cells have been retrieved, Fourier transformations and employed to compute the response of the complete domain in space domain:

$$\hat{u}(x,y,z,\omega)=\frac{1}{2\pi}\int_{-\infty}^{\infty}\tilde{u}_n(x,y,z,k_1,\omega)e^{ik_1x}dk_1 \quad (7)$$

in where $\hat{u}$ is the displacement of the complete domain, and the notation '^' describes the space-frequency domain (x,ω).

3 APPLICATION

The combined DM and 3D FE-PML are employed to simulate the dynamic track-ground behavior. To do so, a ballasted track resting on a semi-infinite soil is considered. Table 1 shows the main properties of the various track components, including the material and dimensions of the rail section, railpad, sleeper, ballast, sub-ballast, and the subgrade. The reference cell of length *d=0.6m* is defined through 8-node solid elements.

Component	Parameter	Value
Track	Gauge	0.7175m
Rail	Section	CEN60/60E2
	Height	0.218m
	Width	0.035m
	Density	7850kg/m^3
	Young's modulus	210GPa
Railpad	Height	0.01m
	Density	1000kg/m^3
	Young's modulus	300MPa
	Poisson's ratio	0.45
	Loss factor	0.15
Sleeper	Material	Concrete
	Depth	0.2m
	Thickness	0.2m
	Length	1.3m
Ballast	Depth	0.3m
	Length (top)	1.6m
	Length (bottom)	2.1m
	Density	1700kg/m^3
	Young's modulus	220MPa
	Poisson's ratio	0.3
	Loss factor	0.4
Sub-ballast	Depth	0.2m
	Length	2.7m
	Density	1900kg/m^3
	Young's modulus	200MPa
	Poisson's ratio	0.3
	Loss factor	0.1
Subgrade	Depth	∞
	Density	1800kg/m^3
	Young's modulus	80MPa
	Poisson's ratio	0.35
	Loss factor	0.1

Table 1: Track properties.

In addition, the reference cell is subject to a stationary impulse force *F* of unit magnitude, $P = 1N$, excited at frequency ω:

$$F(x) = P\delta(x - x_o)e^{i\omega t} \tag{8}$$

where δ is the Dirac delta function defining the impulse, t is the time, and x_o is the observation point. F is applied on the rail above the sleeper support and deflections and velocities are obtained at different positions of the track (see Figure 3):

- the rail on support – i.e. same position of the force,
- the rail at mid-span – i.e. between two sleepers, and
- at the middle of the sleeper.

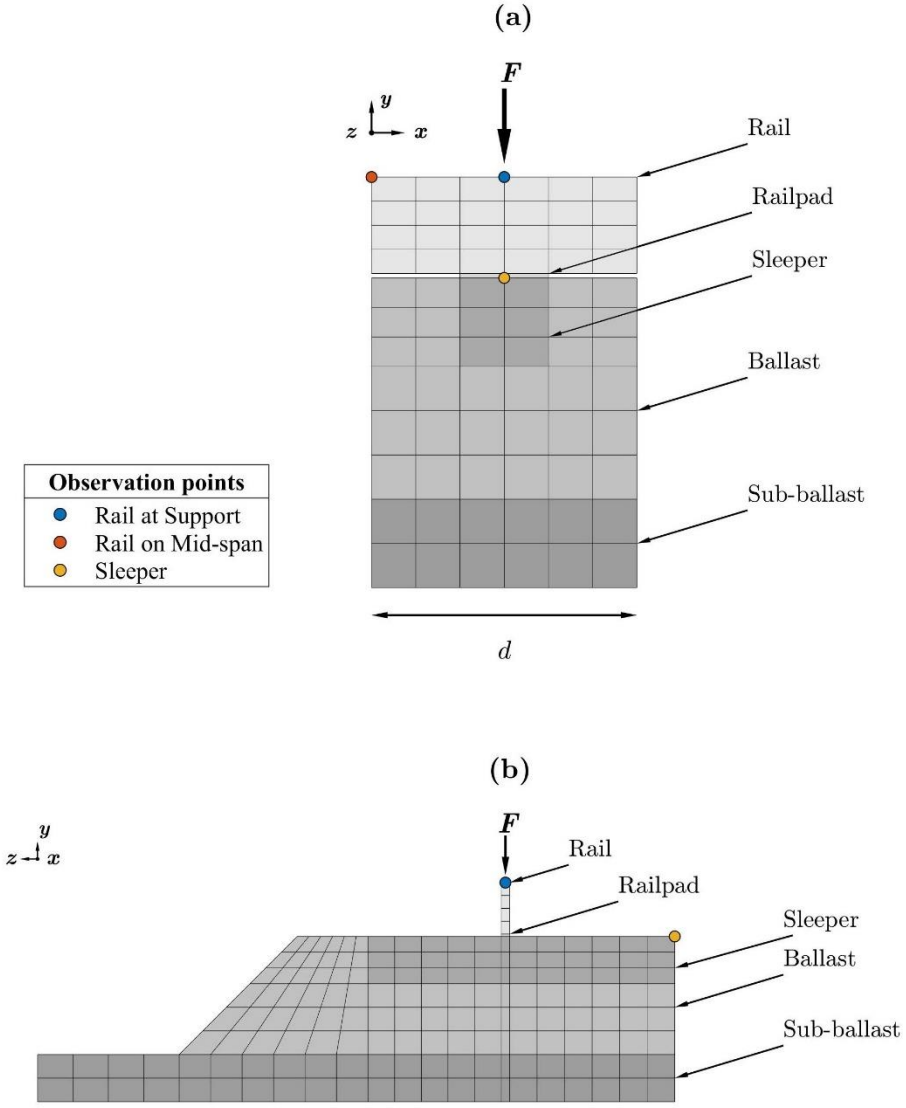

Figure 3: Excitation and observation locations within the model: (a) $x-y$ view, and (b) $y-z$ view. Subgrade layer omitted for visibility.

4 RESULTS

Figure 4 presents the absolute deflection, in the space-frequency domain, at different track positions due to a unit harmonic excitation. Three main regions, corresponding to the frequencies of resonances describe the vibration modes of the total structure: the full-track ($f_{\text{full-track}}$), the railpad (f_{railpad}) and the pin-pin ($f_{\text{pin-pin}}$) resonant frequencies. The first one, corresponding to $f_{\text{full-track}}$, occurs below 20Hz. It can be seen that regardless of the observation point, the maximum deflection is achieved around this frequency. This is consequence of the soft subgrade supporting the much stiffer ballasted track. The soil properties effect decreases with the

frequency until reaching f_{railpad}. At this frequency, the railpad behavior dominates the response. Note that, besides the highlighted frequencies, some other maximum peaks are observed, however, they are result of the wave propagation of the subgrade. Finally, the peak occurring around 1000Hz corresponds to $f_{\text{pin-pin}}$. Since the excitation is applied on the rail above the sleeper support, the peak is downward, resulting in an anti-resonance.

Similar results are observed in the velocity curves of Figure 5. Again, the three main frequencies are visible; however, the response is computed in terms of velocity rather than displacements, leading to a maximum response occurring at high-frequency ranges.

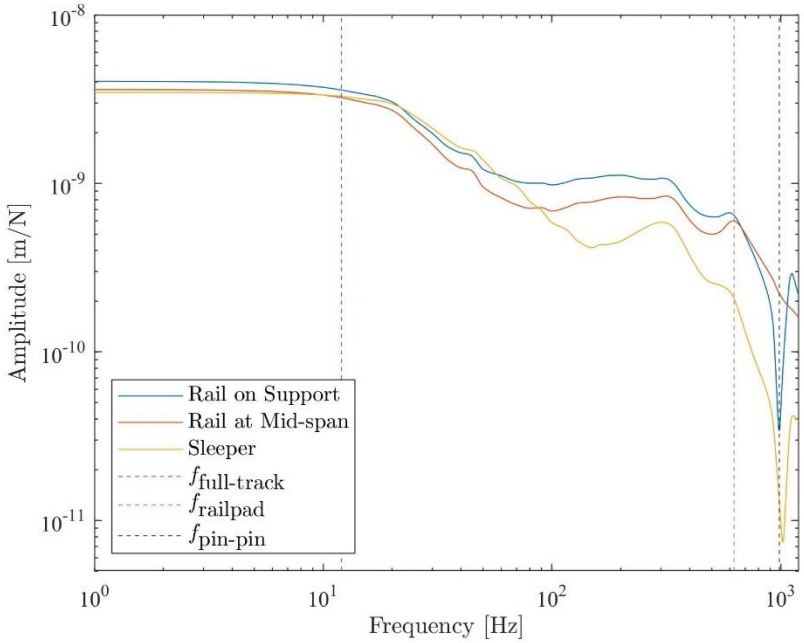

Figure 4: Track deflections due to unit harmonic force *F*.

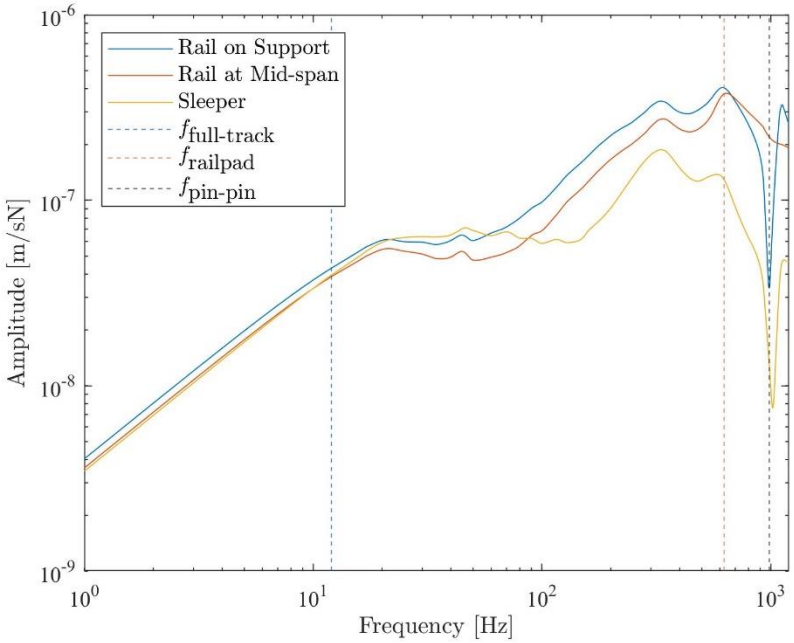

Figure 5: Track velocities due to unit harmonic force *F*.

Figure 6 shows the vibration modes of the track at the tree main frequencies. Figure 6(a) shows that at $f_{\text{full-track}}$, the rail and the sleeper mass move vertically, and in phase, over the ballast. In contrast, in the track behavior corresponding to f_{railpad}, both the rail and the sleeper move in antiphase on the railpad – see Figure 6(b). Similarly, at $f_{\text{pin-pin}}$, the rail and the sleeper are moving in antiphase; however, the wavelength of the rail is described by the support spacing– see Figure 6(c). Overall, in both f_{railpad} and $f_{\text{pin-pin}}$, the rail is vibrating on the supports.

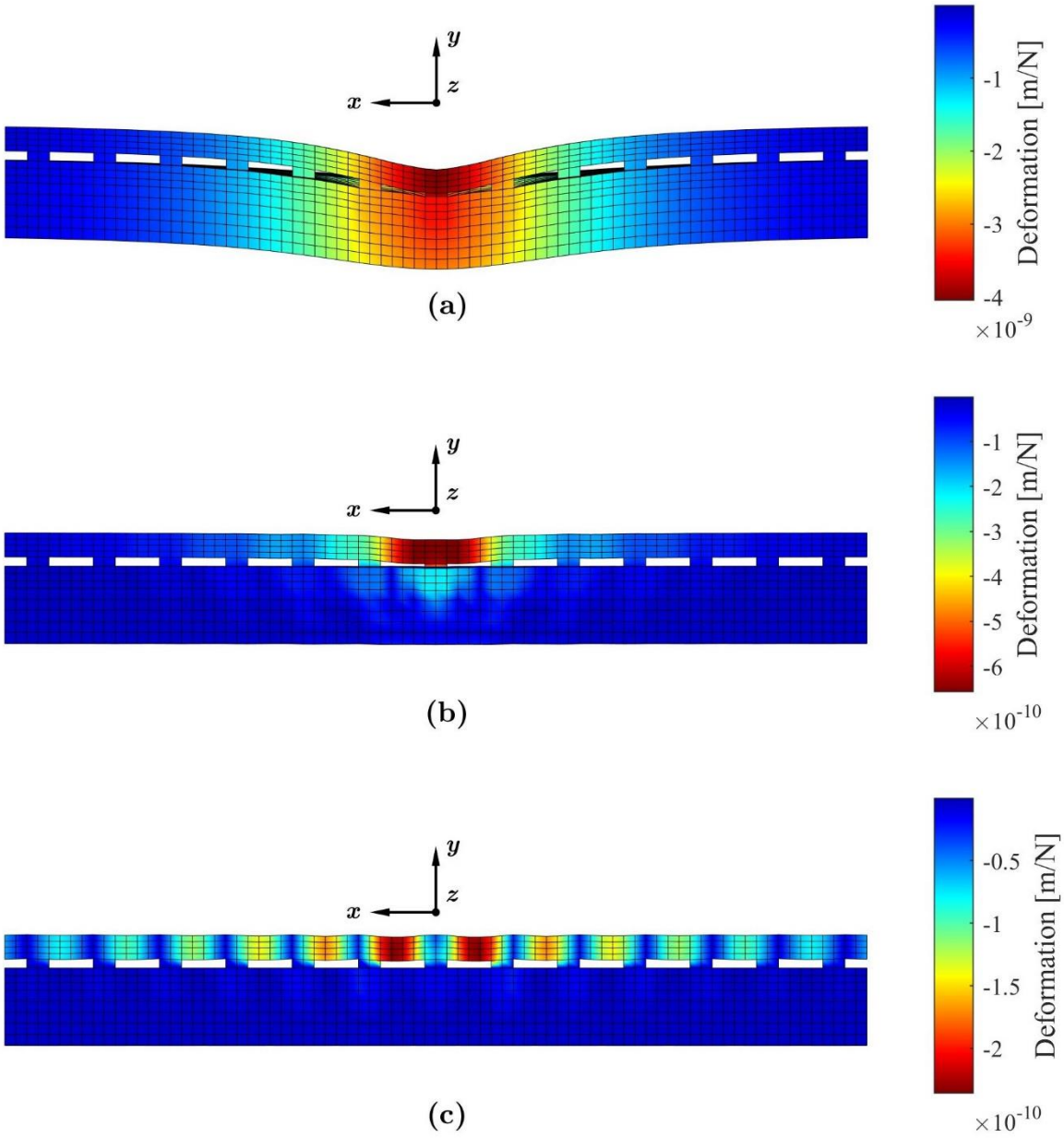

Figure 6: Absolute track response at: (a) full-track resonance (b) railpad resonance, and (c) pin-pin resonance – railpad dimensions and deflections magnified for visibility.

Alternatively, Figure 7(a) and Figure 7(b) present the structure's response, including the subgrade's, around 100 and 325Hz, respectively. It can be noted that although maximum values occur around these frequency values, they do not correspond to the main three resonant frequencies. In both cases, wave propagation is observed within the soil, indicating its properties' influence on the response. However, in the latter, the soil effect reduces since the frequency is

high and closer to the railpad frequency of resonance. In addition, the lower track layers (i.e. ballast and sub-ballast) also affect the total response at 325Hz – see Figure 7(b). It should be noted that, for improved visibility, the railpad dimensions and the deflection values have been magnified in Figures 6 and 7. Additionally, only 13 cells are displayed, i.e. $n = -6{:}\,6$.

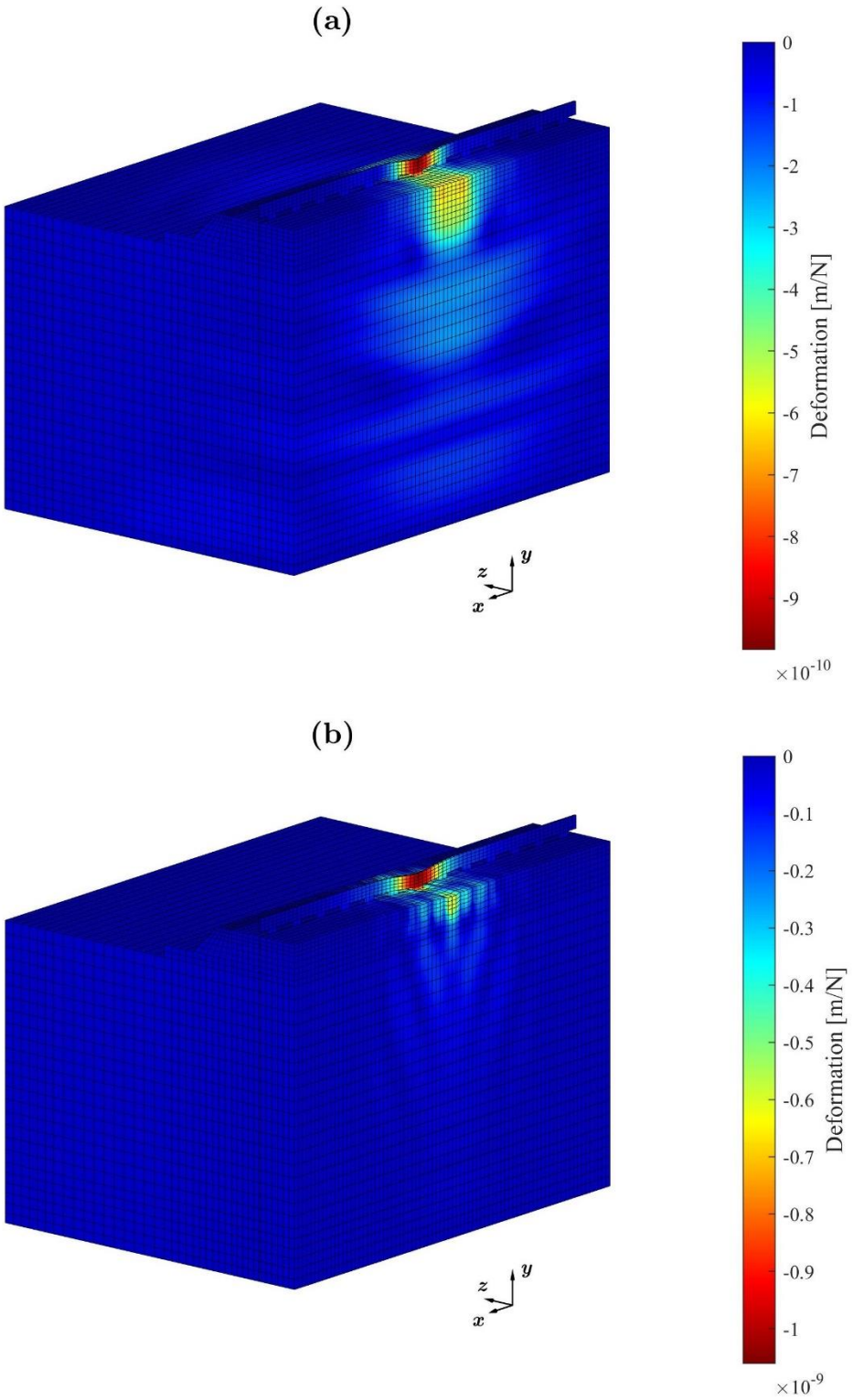

Figure 7: Absolute track response at: (a) 100Hz, and (b) 325Hz – railpad dimensions and deflections magnified for visibility.

5 CONCLUSIONS

Vibration issues in railway systems are caused by the complex dynamic interactions between the train, the track, and the underlying soil. With the growing demand for transportation, so is the severity of these problems, resulting in faster track deteriorations and higher maintenance costs. This has led to the development of simulation techniques to approximate the system's behavior and asses this vibration issues. Thus, this paper employs a direct periodic strategy combined with 3D FE and PML to study a ballasted track resting on a homogeneous soil. The periodic nature of the track is exploited, resulting in a computationally efficient method that only requires the discretization of a slice, which can retrieve the total response.

It can be seen that the DM successfully captures the main resonant frequencies exciting the railway system, including the full-track, railpad and the pin-pin. Since the pin-pin frequency can be simulated, so is its discrete support. Similarly, by combining it with PML, the DM can retrieve the wave propagation effect as described by the vibration modes of the structure. Overall, the obtained results, show that the soil properties play an important role in the track response at lower frequencies. In contrast, higher frequencies results are mostly affected by the track behavior.

REFERENCES

[1] A.P. de Man, Pin-pin resonance as a reference in determining ballasted railway track vibration behaviour. *HERON*, **45**, 35-51, 2000.

[2] A.C. Lamprea-Pineda, D.P. Connolly, M.F.M. Hussein, Beams on elastic foundations – A review of railway applications and solutions. *Transportation Geotechnics*, **33**, 100696, 2022.

[3] K.L. Knothe, S.L. Grassie, Modelling of Railway Track and Vehicle/Track Interaction at High Frequencies. *Vehicle System Dynamics*, **22**, 209-262, 1993.

[4] S.L. Grassie, R.W. Gregory, D. Harrison, K.L. Johnson. The Dynamic Response of Railway Track to High Frequency Vertical Excitation. *Journal of Mechanical Engineering Science*, **24**, 77-90, 1982.

[5] D. Thompson, *Railway Noise and Vibration, 1st Edition.* Elsevier, 2009.

[6] X. Sheng, C.J.C. Jones, M. Petyt, Ground vibration generated by a harmonic load acting on a railway track. *Journal of Sound and Vibration*, **225**, 3–28, 1999.

[7] X. Sheng, C.J.C. Jones, M. Petyt, Ground vibration generated by a load moving along a railway track. *Journal of Sound and Vibration*, **228**, 129–56, 1999.

[8] E. Kausel, Thin-layer method: Formulation in the time domain. *International Journal for Numerical Methods in Engineering*, **37**, 927–941, 1994.

[9] Y. Ma, V.L. Markine, A.A. Mashal, M. Ren, Effect of wheel–rail interface parameters on contact stability in explicit finite element analysis. *Proceedings of the Institution of Mechanical Engineers, Part F: Journal of Rail and Rapid Transit*, **232**, 1879–1894, 2018.

[10] H. Wang, V. Markine, Modelling of the long-term behaviour of transition zones: Prediction of track settlement. *Engineering Structures*,**156**, 294–304, 2018.

[11] P. Chumyen, D.P. Connolly, P.K. Woodward, V. Markine. The effect of soil improvement and auxiliary rails at railway track transition zones. *Soil Dynamics and Earthquake Engineering*, **155**, 107200, 2022.

[12] E. Arlaud, S. Costa D'Aguiar, E. Balmes, Receptance of railway tracks at low frequency: Numerical and experimental approaches. *Transportation Geotechnics*, **9**, 1–16, 2016.

[13] M, Germonpré, G, Degrande, G, Lombaert, A track model for railway-induced ground vibration resulting from a transition zone. *Proceedings of the Institution of Mechanical Engineers, Part F: Journal of Rail and Rapid Transit*, **232**, 1703–1717, 2018.

[14] P. Ferreira, Modelling and prediction of the dynamic behaviour of railway infrastructures at very high speeds. *Universidade Técnica de Lisboa, Instituto Superior Técnico*, 1-432, 2010.

[15] B.R. Mace, D. Duhamel, M.J. Brennan, L. Hinke, Finite element prediction of wave motion in structural waveguides. *The Journal of the Acoustical Society of America*, **117**, 2835–2843, 2005.

[16] M. Sadri, T. Lu, M. Steenbergen, Railway track degradation: The contribution of a spatially variant support stiffness - Local variation. *Journal of Sound and Vibration*, **455**, 203–20, 2019.

[17] M. Sadri, T. Lu, M. Steenbergen, Railway track degradation: The contribution of a spatially variant support stiffness - Global variation. *Journal of Sound and Vibration*, **464**, 114992, 2020.

[18] S. Gupta, G. Degrande, H. Chebli, D. Clouteau, M.F.M. Hussein, H.E.M. Hunt. A coupled periodic FE-BE model for ground-borne vibrations from underground railways. *III European Conference on Computational Mechanics (ECCM-2006)*, Lisbon, Portugal, June 5–9, 2006.

[19] H. Chebli, R. Othman, D. Clouteau, M. Arnst, G. Degrande, 3D periodic BE–FE model for various transportation structures interacting with soil. *Computers and Geotechnics*, **35**, 22–32, 2008.

[20] M.F.M. Hussein, H.E.M. Hunt, Modelling of Floating-Slab Track with Discontinuous Slab: Part 1: Response to Oscillating Moving Loads. *Journal of Low Frequency Noise, Vibration and Active Control*, 25, 23–39, 2006.

[21] J.A. Forrest, Modelling of Ground Vibration from Underground Railways. *University of Cambridge*, 1999.

[22] P. Alves Costa, R. Calçada, A. Silva Cardoso, Track–ground vibrations induced by railway traffic: In-situ measurements and validation of a 2.5D FEM-BEM model. *Soil Dynamics and Earthquake Engineering*, **32**,111–28, 2012.

[23] P. Alves Costa, R. Calçada, A. Silva Cardoso, Ballast mats for the reduction of railway traffic vibrations, Numerical study. *Soil Dynamics and Earthquake Engineering*, **42**, 137–50, 2012.

[24] C. Charoenwong, D.P. Connolly, P.K. Woodward, P. Galvín, P. Alves Costa, Analytical forecasting of long-term railway track settlement. *Computers and Geotechnics*, **143**, 104601, 2022.

[25] C. Charoenwong, D.P. Connolly, K. Odolinski, P. Alves Costa, P. Galvín, A. Smith, The effect of rolling stock characteristics on differential railway track settlement: An engineering-economic model. *Transportation Geotechnics*, **37**, 100845, 2022.

[26] C. Charoenwong, D.P. Connolly, A. Colaço, P. Alves Costa, P.K. Woodward, A. Romero, P. Galvín, Railway slab vs ballasted track: a comparison of track geometry degradation. *Construction and Building Materials*, 2023.

[27] J. Fernández Ruiz, P.J. Soares, P. Alves Costa, D.P. Connolly, The effect of tunnel construction on future underground railway vibrations. Soil Dynamics and Earthquake Engineering, 125, 105756, 2019.

[28] D.P. Connolly, A. Giannopoulos, M.C. Forde, A higher order perfectly matched layer formulation for finite-difference time-domain seismic wave modeling. *GEOPHYSICS*, **80**, T1–16, 2015.

[29] A. Castanheira-Pinto, A. Colaço, J.F. Ruiz, P. Alves Costa, L. Godinho, Simplified approach for ground reinforcement design to enhance critical speed. *Soil Dynamics and Earthquake Engineering*, **153**, 107078, 2022.

[30] P. Gómez García, J.P. Fernández-Álvarez, Floquet-Bloch Theory and Its Application to the Dispersion Curves of Nonperiodic Layered Systems. *Mathematical Problems in Engineering*, **2015**, 1–12, 2015.